# Towards Nanoscale Molecular Analysis at Atmospheric Pressure by a Near-Field Laser Ablation Ion Trap/Time-of-Flight Mass Spectrometer

**ARTICLE** *in* ANALYTICAL CHEMISTRY · AUGUST 2008

Impact Factor: 5.64 · DOI: 10.1021/ac8005044 · Source: PubMed



**5 AUTHORS**, INCLUDING:

Gerardo Gamez
Texas Tech University
**68** PUBLICATIONS **2,166** CITATIONS
SEE PROFILE

Renato Zenobi
ETH Zurich
**459** PUBLICATIONS **13,155** CITATIONS
SEE PROFILE

*Anal. Chem.* **2008,** *80,* 6537–6544

# Towards Nanoscale Molecular Analysis at Atmospheric Pressure by a Near-Field Laser Ablation Ion Trap/Time-of-Flight Mass Spectrometer

**Thomas A. Schmitz, Gerardo Gamez, Patrick D. Setz,† Liang Zhu, and Renato Zenobi***

*Department of Chemistry and Applied Biosciences, ETH Zurich, 8093 Zurich, Switzerland*

**An instrument that combines near-field laser ablation at atmospheric pressure with an ion trap/time-of-flight mass spectrometer was developed. By coupling a UV laser into a fiber tip of a scanning near-field optical microscope, ablation craters much smaller than achievable with conventional laser optics can in principle be obtained. Laser ablation was performed on samples such as DHB, anthracene, and pyrene. Desorbed neutral analytes are transferred from atmospheric pressure to an ion trap, ionized, and stored. After 10 ms, the ions are extracted into a sensitive time-of-flight spectrometer. We demonstrate the feasibility of this unique SNOM-MS instrument for chemical analysis with unprecedented lateral resolution at atmospheric pressure. Spatially resolved molecular analysis with a lateral resolution of 5 $\mu$m (fwhm) and a sensitivity of ~60 fmol of solid anthracene is demonstrated, along with topographical analysis with the same instrument. No other technique available today offers this lateral resolution in combination with soft mass spectrometry and the capability of sampling fragile specimens at atmospheric pressure.**

Materials and structures on the micro- and nanometer scale have become of great interest and relevance in modern science and engineering. For chemical analysis, however, this field poses major challenges: most traditional molecular analysis methods are far from having the required lateral resolution, and most techniques used for nanoscale characterization, such as atomic force microscopy, scanning tunneling microscopy, or scanning electron microscopy (SEM) yield only very limited or no chemical information. Nevertheless, the interest in studying biological samples with scanning probe methods (SPM) has greatly grown over the past few years, and open questions in the fields of proteomics, membrane function, and cell biology are beginning to be addressed by nanoanalytical methods.[1,2] At the same time, spatially resolved molecular analysis using imaging mass spectrometry has become an important tool.[3]

The molecular analysis of fragile compounds in complex mixtures or specimens (such as in biological systems) requires highly specific and sensitive analytical methods, preferably requiring little or no sample preparation. Atmospheric pressure (AP) mass spectrometry, which is especially suitable for such tasks, has been advanced enormously in recent years and has enriched the analytical instrumental portfolio with a great variety of novel ion sources. AP methods have origins dating back over 30 years with the invention of atmospheric pressure chemical ionization (APCI)[4] and gained thrust with the invention of electrospray ionization (ESI).[5] While APCI and ESI are restricted to the analysis of liquid samples at atmospheric pressure, advances in recent years have added descendant sources that allow soft molecular analysis of surfaces at atmospheric pressure: direct analysis in real time,[6] desorption electrospray ionization (DESI),[7] desorption atmospheric pressure chemical ionization, and neutral desorption extractive electrospray ionization,[9] to name a few. Biological imaging with 300−400-$\mu$m lateral resolution was demonstrated recently with DESI.[10] The ability to image fragile biological systems such as tissues or live cells at atmospheric pressure is compelling, as preparation and handling of biological specimens for analysis in vacuum is often difficult, time-consuming, or even impossible (in the case of in vivo analysis). Because individual cells typically have sizes in the range of 15−30 $\mu$m, the ambient ionization methods mentioned above do not yet have a suitable lateral resolution for the analysis of single cells, not to speak of subcellular compartments. Our goal was therefore to build a mass spectrometer with an AP interface that allows direct analysis of solid samples at atmospheric pressure with very high lateral resolution, which can be achieved using laser ablation.

Spatial resolution in the range of 50−100 $\mu$m can routinely be achieved with laser ablation MS techniques, of which matrix-assisted laser ablation (MALDI) is the workhorse in bioanalysis

* To whom correspondence should be addressed. Fax: +41-44-632-1292. E-mail: zenobi@org.chem.ethz.ch.

† Current address: Clinical Chemistry, University Hospital Zurich, Rämistr. 100, CH-8091 Zurich, Switzerland.

(1) Poggi, M. A.; Gadsby, E. D.; Bottomley, L. A.; King, W. P.; Oroudjev, E.; Hansma, H. *Anal. Chem.* **2004**, *76*, 3429–3443.

(2) Takano, H.; Kenseth, J. R.; Wong, S. S.; O'Brien, J. C.; Porter, M. D. *Chem. Rev.* **1999**, *99*, 2845–2890.

(3) McDonnell, L. A.; Heeren, R. M. A. *Mass Spectrom. Rev.* **2006**, *26*, 606–643.

(4) Horning, E. C.; Horning, M. G.; Carroll, D. I.; Dzidic, I.; Stillwell, R. N. *Anal. Chem.* **1973**, *45*, 936.

(5) Fenn, J. B.; Mann, M.; Meng, C. K.; Wong, S. F.; Whitehouse, C. M. *Science* **1989**, *246*, 64–71.

(6) Cody, R. B.; Laramee, J. A.; Durst, H. D. *Anal. Chem.* **2005**, *77*, 2297–2302.

(7) Takats, Z.; Wiseman, J. M.; Gologan, B.; Cooks, R. G. *Science* **2004**, *306*, 471–473.

(8) Takats, Z.; Cotte-Rodriguez, I.; Talaty, N.; Chen, H. W.; Cooks, R. G. *Chem. Commun.* **2005**, 1950–1952.

(9) Chen, H. W.; Venter, A.; Cooks, R. G. *Chem. Commun.* **2006**, 2042–2044.

(10) Ifa, D. R.; Wiseman, J. M.; Song, Q. Y.; Cooks, R. G. *Int. J. Mass Spectrom.* **2007**, *259*, 8–15.

10.1021/ac8005044 CCC: $40.75 
Published on Web 07/12/2008

and proteomics. While MALDI and other laser ablation techniques traditionally require the sample to be in high vacuum, atmospheric pressure MALDI using ultraviolet laser light has been demonstrated[11] with a spot size of ~1 mm and a detection limit of <100 fmol for peptides. Also, IR-MALDI can be performed at atmospheric pressure, which was demonstrated first using a water/glycerol matrix[12] and recently without the addition of a MALDI-matrix.[13] In succession to the latter work, the group of Vertes[14] combined the ~0.4-mm spatial resolution of laser ablation with the virtues of atmospheric electrospray ionization, yielding a new approach for matrix-free mid-IR imaging at atmospheric pressure. Detection limits as low as 8 fmol and an upper mass limit of 66 kDa were reported, clearly exceptional figures of merit for an atmospheric pressure MS imaging technique. In laser ablation, lateral resolution is determined by the laser spot size, which depends on the laser wavelength and optics. Using oversampling techniques with appropriate data processing, 25−40-$\mu$m resolution can be achieved in UV MALDI without physically reducing the laser spot size.[15]

Theoretically, laser ablation spots could be focused to much smaller size, given that the fundamental physical limit of diffraction ($\sim\lambda/2$) would allow a focal diameter as small as ~175 nm (for a mid-UV laser) or ~1.5 $\mu$m (for a mid-IR laser), respectively. In principle, laser ablation MS at atmospheric pressure should thus be possible with sub-10 $\mu$m resolution, but this has never been demonstrated. Better spatial resolution has so far only been achieved in high-vacuum systems. For example, sophisticated optical arrangements such as the combination of confocal microscopy and MS (SMALDI) by the group of Spengler achieved a resolution for laser ablation MS down to 0.6 $\mu$m.[16,17] In a recent study, MALDI-MS imaging of high molecular mass compounds up to 27 000 $m/z$ was successfully demonstrated for laser spot sizes of 6−10-$\mu$m diameter using a similar concept of highly focused coaxial laser illumination.[18] Also, "stigmatic ion imaging" has been demonstrated using a mass spectrometer with a position-sensitive detector in "microscope" mode, which gives a spatial resolution of 2−4 $\mu$m.[19] Another competing technique with excellent spatial resolution is secondary-ion mass spectrometry (SIMS), especially since its mass range was extended to up to $m/z$ 2500 due to recent advances.[20] SIMS routinely allows imaging with 100−200-nm lateral resolution and can reach down to 30-nm spatial resolution[21] but requires ultrahigh vacuum systems. Furthermore, in SIMS imaging a compromise has to be found between a tightly focused primary ion beam for achieving high spatial resolution, resulting in molecular fragmentation ("dynamic" mode SIMS), and the ability to reach a high upper $m/z$ limit by keeping molecules intact ("static" SIMS using a defocused beam, resulting in much lower resolution). An overriding issue is that a smaller spot size in microprobe MS invariably leads to a smaller amount of material available for analysis, resulting in a inferior limit of detection. For example, apart from the fact that ionization efficiencies are ≪100%, the amount of material from a laser ablation crater in the 100 nm−1 $\mu$m diameter range is on the order of a few attomoles to a few femtomoles, depending on the material and laser ablation depth, requiring a very high sensitivity mass spectrometer.

While all conventional optical techniques are ultimately diffraction-limited, scanning near-field optical microscopy (SNOM)[22] can break the diffraction limit and is especially useful in the biological sciences, for example, for nanoscale fluorescence imaging.[23,24] In the 1990s, our group demonstrated that the basic principle of a SNOM, which can be compared to a nano light source, can be also employed for pulsed UV laser ablation, producing craters as small as 70 nm.[25,26] Kossakovski et al. published the first combination of laser ablation in the near field with MALDI mass spectrometry in a high-vacuum system, reaching a lateral resolution of 1 $\mu$m.[27] In 2001, we demonstrated for the first time that near-field laser ablation at atmospheric pressure can be coupled to mass spectrometry, yielding a lateral resolution of ~170 nm, and a sensitivity in the low attomole range. Despite these impressive figures of merit, that experiment had severe limitations: a simple residual gas analyzer consisting of an electron impact (EI) ionization source and a quadrupole mass spectrometer (QMS) was used. The QMS was too slow to acquire full mass spectra while the 100-ms material transient from the pulsed near-field laser ablation reached it. Only single-mass traces were therefore reported. The atmospheric sampling interface was also very simple. It consisted of a 20-$\mu$m-diameter capillary inlet connected to a tapered stainless steel tube, which led directly to the EI source. Since the 20-$\mu$m capillary was prone to clogging, it was difficult to work with laser ablation from solids. Instead, a gaseous photodecomposition product from a triazene dimer, $N_2$, was successfully monitored. Obviously, it is rather straightforward to sample, ionize, and detect gaseous $N_2$ with very high efficiency.

In contrast to a quadrupole, a time-of-flight (TOF) mass analyzer offers fast acquisition, high ion transmission, and quasi-simultaneous mass analysis with reasonable resolution over the entire $m/z$ range. However, a direct coupling of atmospheric pressure near-field laser ablation to a TOF is not feasible due to the temporal spread of the neutral ablation products as they reach the ion source. Therefore, a preconcentration step between laser ablation and mass separation is necessary. In this work, an ion trap/TOF instrument is introduced for precisely this purpose. After having accumulated the ions of interest within the ion trap,


(11) Laiko, V. V.; Baldwin, M. A.; Burlingame, A. L. *Anal. Chem.* **2000**, *72*, 652–657.
(12) Laiko, V. V.; Taranenko, N. I.; Berkout, V. D.; Yakshin, M. A.; Prasad, C. R.; Lee, H. S.; Doroshenko, V. M. *J. Am. Soc. Mass. Spectrom.* **2002**, *13*, 354–361.
(13) Li, Y.; Shresta, B.; Vertes, A. *Anal. Chem.* **2007**, *79*, 523–532.
(14) Nemes, P.; Vertes, A. *Anal. Chem.* **2007**, *79*, 8098–8106.
(15) Jurchen, J. C.; Rubakhin, S. S.; Sweedler, J. V. *J. Am. Soc. Mass. Spectrom.* **2005**, *16*, 1654–1659.
(16) Spengler, B.; Hubert, M. *J. Am. Soc. Mass. Spectrom.* **2002**, *13*, 735–748.
(17) Bouschen, W.; Spengler, B. *Int. J. Mass Spectrom.* **2007**, *266*, 129–137.
(18) Chaurand, P.; Schriver, K. E.; Caprioli, R. M. *J. Mass Spectrom.* **2007**, *42*, 476–489.
(19) Luxembourg, S. L.; Mize, T. H.; McDonnell, L. A.; Heeren, R. M. A. *Anal. Chem.* **2004**, *76*, 5339–5344.
(20) Touboul, D.; Halgand, F.; Brunelle, A.; Kersting, R.; Tallarek, E.; Hagenhoff, B.; Laprevote, O. *Anal. Chem.* **2004**, *76*, 1550–1559.
(21) Slodzian, G.; Daigne, B.; Girard, F.; Boust, F.; Hillion, F. *Biol. Cell* **1992**, *74*, 43–50.
(22) Betzig, E.; Trautman, J. K.; Harris, T. D.; Weiner, J. S.; Kostelak, R. L. *Science* **1991**, *251*, 1468–1470.
(23) Dunn, R. C. *Chem. Rev.* **1999**, *99*, 2891–2992.
(24) Gao, H.; Oberringer, M.; Englisch, A.; Hanselmann, R. G.; Hartmann, U. *Ultramicroscopy* **2001**, *86*, 145–150.
(25) Zeisel, D.; Nettesheim, S.; Dutoit, B.; Zenobi, R. *Appl. Phys. Lett.* **1996**, *68*, 2491–2492.
(26) Dutoit, B.; Zeisel, D.; Deckert, V.; Zenobi, R. *J. Phys. Chem. B* **1997**, *101*, 6955–6959.
(27) Kossakovski, D. A.; O'Connor, S. D.; Widmer, M.; Baldeschwieler, J. D.; Beauchamp, J. L. *Ultramicroscopy* **1998**, *71*, 111–115.

they are extracted in a pulsed fashion into the field-free TOF region, therefore yielding a better limit of detection for the overall laser ablation-MS process. Another aspect, which should improve the limit of detection in our system, is that neutral species from the laser ablation are sampled at atmospheric pressure, transported as neutrals into the vacuum, and only ionized in the ion trap. This is because laser ablation and MALDI processes are fairly ineffective in producing ions, as ion-to-neutrals ratios for UV laser desorption in the range of 1:1000 to 1:10 000 are reported.[28,29] Much of the ablated material would therefore be "wasted" if one would only sample the ionized species produced during the laser ablation process.

Here, we present the experimental realization of atmospheric pressure near-field ablation-MS and demonstrate the feasibility of obtaining molecular mass spectra from molecular solids. Our instrument allows mass analysis of a wide $m/z$ range for laser ablation at atmospheric pressure with a resolution in the low-micrometer range, which has never been achieved before. Moreover, it incorporates topographical surface scanning with the same hardware.

## EXPERIMENTAL SECTION

**Chemicals and Materials.** Unless otherwise noted, all chemicals and materials were purchased at the highest available quality from Fluka (Buchs, Switzerland) and used without any further purification. Pyrene (98%) was bought from Acros Organics (Geel, Belgium); chromium chunks (99.99% purity, metals basis) and aluminum wire (99.999%, metals basis) were obtained from Alfa Aesar (Karlsruhe, Germany).

**Scanning Near-Field Optical Microscopy.** A commercial SNOM instrument (Topometrix Lumina, Veeco Metrology Inc., Santa Barbara CA) was used together with SPMLab 6.02 for instrument control and data acquisition. Our instrument is equipped with a noncontact shear-force scan head with a maximum piezo range of $100 \times 100$ $\mu$m for tip scanning. The acquired data were further processed by SPIP (Image Metrology, Hørsholm, Denmark) or Gwyddion (http://gwyddion.net).

**SNOM Probes.** The SNOM tips used for SNOM-MS laser ablation were fabricated by the "tube etching" method, which was described previously by our group.[30] A multimode silica fiber with good UV transmission (attenuation 70 dB/km at 350 nm) was used as raw material for all SNOM tips produced (Superguide G fiber, High-OH, type SFS50/125Y, multimode UV−vis, 0.22 NA, 50-$\mu$m core diameter, 125-$\mu$m cladding diameter, 250-$\mu$m acrylate jacket, from Fiberguide Industries, Stirling NJ). Following taper formation by etching in 40% HF with an overlayer of isooctane for 120 min, the acrylate fiber jacket was removed by hot $H_2SO_4$, and the fiber was washed with ethanol and deionized water and then dried. The tip was coated in a vacuum evaporation chamber (MED-020, Bal-Tec, Balzers, Principality of Liechtenstein) with layers of aluminum and chromium, as published previously,[31] in order to obtain tips with an optimized damage threshold. The tips were glued onto

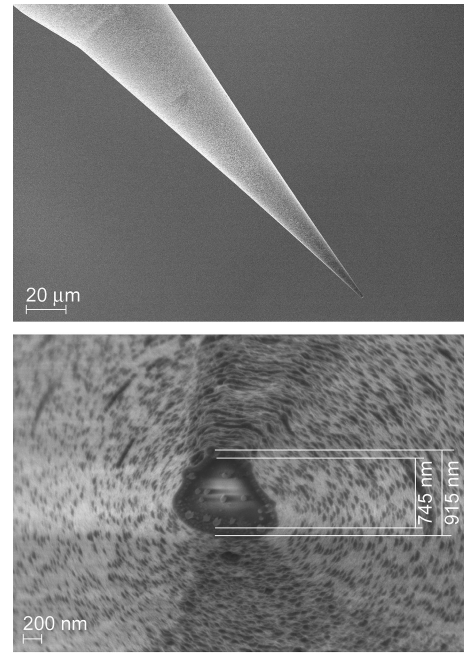


**Figure 1.** Typical SNOM tip for near-field laser ablation, imaged with scanning electron microscopy. The top image is an overview showing the step between inner- and outer-fiber core as well as the overall smoothness of the Al/Cr coating. The bottom image is a closeup, showing the aperture shape and size (~745 nm).

modified tuning-fork assemblies whose oscillator was extracted out of standard 32.768-kHz watch crystals (AEL Crystals, West Sussex, United Kingdom). Figure 1 shows a typical SNOM tip used for near-field laser ablation MS, with a relatively large aperture size (500−800 nm). Although apertures sizes smaller than 100 nm would be possible to produce, the amount of ablated material then available for analysis would be much smaller, challenging the current limit of detection of our instrument.

**Ion Trap/Time-of-Flight Mass Spectrometry (IT-TOF-MS).** The MS used is a home-built IT-TOF that has an atmospheric pressure sampling interface for neutral molecules. Briefly, as this instrument already has been presented in the literature,[32] only recent modifications will be described in some detail here. The atmospheric pressure interface was modified for the SNOM-MS application. Instead of a two-stage pressure reducing interface, a one-stage design with only one nozzle−skimmer pair was used. An intermediate-polarity deactivated fused-silica GC guard column with an inner diameter of 250 $\mu$m was used as capillary for sampling at atmospheric pressure. The capillary was held in a metal shaft heated to 170−200 °C on a length of 18 cm between the sampling "orifice" and the exit nozzle in the intermediate-pressure manifold. Two rough pumps with a total pump speed of 13 L/s connected to the intermediate stage achieved a pressure of typically 0.3−0.4 mbar in this stage, and a vacuum of $5 \times 10^{-6}$ to $2 \times 10^{-6}$ mbar was maintained in the main ion trap chamber by an oil diffusion pump for a leak rate of 34−42 cm$^3$/min, which was largely determined by the skimmer−nozzle distance. The setup was also modified such that sample vapor entered the ion trap through a 0.6-mm hole in the central ring electrode, perpendicular to the IT-TOF axis. Figure 2 (left side) shows the IT-TOF setup used in this work.

(28) Ens, W.; Mao, Y.; Mayer, F.; Standing, K. G. *Rapid Commun. Mass Spectrom.* **1991**, *5*, 117–123.
(29) Mowry, C. D.; Johnston, M. V. *Rapid Commun. Mass Spectrom.* **1993**, *7*, 569–575.
(30) Stöckle, R.; Fokas, C.; Deckert, V.; Zenobi, R.; Sick, B.; Hecht, B.; Wild, U. P. *Appl. Phys. Lett.* **1999**, *75*, 160–162.
(31) Stöckle, R. M.; Schaller, N.; Deckert, V.; Fokas, C.; Zenobi, R. *J. Microsc.* **1999**, *194*, 378–382.
(32) Setz, P. D.; Schmitz, T. A.; Zenobi, R. *Rev. Sci. Instrum.* **2006**, *77*, 024101.

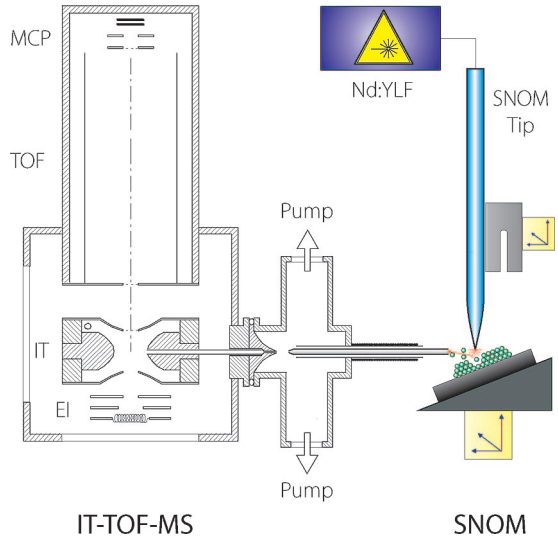


**Figure 2.** Instrumental setup of the SNOM-MS instrument (left part, IT-TOF mass spectrometer; right part, SNOM with UV laser coupled into the SNOM fiber). Ablation takes place in the optical near field on the surface of a sample that is kept at atmospheric pressure/ambient conditions. The ablated neutral species are sampled with a capillary and are transported into the mass spectrometer (not drawn to scale).

In all experiments shown, ionization was performed inside the IT using a coaxial electron impact source, which was gated 15 ms after the first laser shot for a period of 20 ms, followed by a 10-ms storage time of the ionized molecules in the ion trap before extraction into the time-of-flight tube. The trapping rf amplitude was adjusted for optimum stability of the analyte ions (typical rf amplitude: 1000−1500 V peak-peak). By doing so, the highest ion yield for the mass range of interest could be obtained while undesired background below $m/z$ 50−70 was cut off, which also minimizes space-charge effects and maximizes the trap capacity available for analyte ions. Mass spectra are collected on a digital oscilloscope (LC584A, LeCroy, Chestnut Ridge NY) with 2 Gs/s sampling rate that recorded the preamplified transients of the multichannel plate detector.

**SNOM-MS Setup.** The complete setup for SNOM near-field laser ablation mass spectrometry is schematically depicted in Figure 2. It consists of the aforementioned SNOM instrument (right side) and the IT-TOF mass spectrometer (left side of figure).

A frequency-tripled, Q-switched Nd:YLF UV laser (349 nm, <15-ns nominal pulse width) with a repetition rate of up to 2 kHz (Triton, Spectra Physics, Mountain View CA) is coupled into the blunt end of the SNOM fiber, whose sharp tip is kept by shear-force feedback within a 5−15-nm distance of the sample surface. Laser pulse energies (in $\mu$J/pulse) refer to the output of the laser that is coupled into the SNOM fiber, not the output of the SNOM tip. The sample is fixed onto a glass slide on a simple solid sample holder that is tilted by 15° for better sampling efficiency: a tilted surface not only allows positioning the sampling capillary closer to the SNOM tip but also directs the laser ablation plume in a defined direction, where the sampling capillary is then positioned. The coarse positioning of the tip relative to the sample surface is first done manually, and then the fine positioning is achieved by the piezoactuators of the scan head that move the tip. Although our instrument also allows us to scan the sample on a piezotable, this option was not used because it proved to be mechanically problematic with a tilted sample and a sampling capillary in proximity. The sampling capillary could be positioned within 25−100 $\mu$m of the ablation spot using a micromanipulator (Nikon Narishige MO-338, Tokyo, Japan). The relative positioning between sample, SNOM tip, and MS sampling capillary could be observed by two CCD cameras from the side and along the axis of the sampling capillary.

By scanning the tip in shear-force feedback over the sample, topographical images of the sample can be recorded. At a desired location, laser ablation was performed using bursts of laser pulses at a repetition rate of 2 kHz. The ablation plume is sampled and transferred by the heated MS sampling capillary via a intermediate-pressure stage into the IT-TOF.

## RESULTS AND DISCUSSION

**Near-Field Laser Ablation of Solid 2,5-Dihydrobenzoic Acid (DHB) and Anthracene.** Solid crystals of the commonly used MALDI matrix DHB and of anthracene, which both absorb light in the UV, were used for laser ablation in the near field through a SNOM tip. Each surface was first scanned, to obtain a topographic image of the sample. Then, the SNOM tip was manually placed at a desired location where laser ablation was performed. After laser ablation, the surface could be scanned again and the resulting crater be observed (see Figure 3).

The craters shown have top diameters of 1.7 (Figure 3A), 8.5 (Figure 3B), and 1.1 $\mu$m (Figure 3C) and a full width at half-maximum (fwhm) of 0.8, 5.2, and 0.5 $\mu$m, respectively. Not only different crater sizes, which are also caused by the different laser conditions and materials, but also different shapes of the craters can clearly be noted. As the SNOM tips employed were different for each of the examples shown, this explains the different crater shapes. SNOM tips often did not have round apertures but in practice exhibited irregular shapes (see Figure 1). In addition to the data shown, in all three examples, partial redeposition of ablated material occurred, especially in the case of DHB, which has a higher melting point than anthracene. Before laser ablation, the topography in Figure 3C had a $z$-scale range of 25 nm, but after laser ablation it was 200 nm, of which 125 nm is due to the crater depth and the rest due to material being redeposited directly to the right of the center of the crater. Figure 3 also illustrates that optical resolution/lateral resolution of laser ablation and topographic resolution can be very different: While the laser ablation resolution in Figure 3C is ~1 $\mu$m, the topographical resolution is on the order of ≤50 nm. While laser ablation resolution in the near-field is determined by the aperture size and the laser power, topographical resolution can be much higher in the case of protrusions or surface irregularities of the tip, which will act as a "super" tip. This allows a very good topographical characterization of the surface, including the laser ablation craters.

**SNOM-MS of Solid Anthracene.** A single crystal of anthracene was used as a sample for SNOM-MS and the topography was first acquired. While in feedback, 10 bursts of 20 laser shots each were delivered through the SNOM tip, which was parked at a preselected position on the crystal. The laser ablation was synchronized with the IT-TOF mass spectral acquisition: 15 ms after the first laser shot (which corresponds to the minimum dead time for gas-phase sample transport from atmosphere to the IT), the gate of the electron impact source was switched on for 20

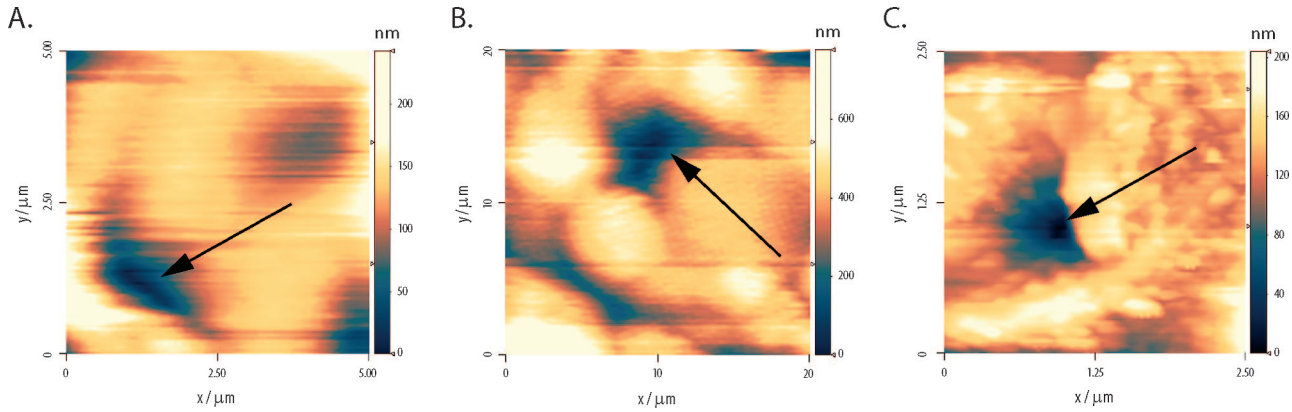


**Figure 3.** (A) Near-field laser ablation craters on a solid DHB crystal surface (11 single shots at 2 kHz, 70 $\mu$J/pulse laser output). (B) Near-field laser ablation on a solid anthracene crystal surface (5 bursts of 10 laser shots at 2 kHz, 30 $\mu$J/pulse laser output). (C) Near-field laser ablation on a solid DHB crystal surface (1 single shot of a VLSI nitrogen laser at 337 nm, 100 $\mu$J/pulse laser output after attenuation). All topographies were obtained by shear-force imaging. Note the different *x*/*y* scan ranges.

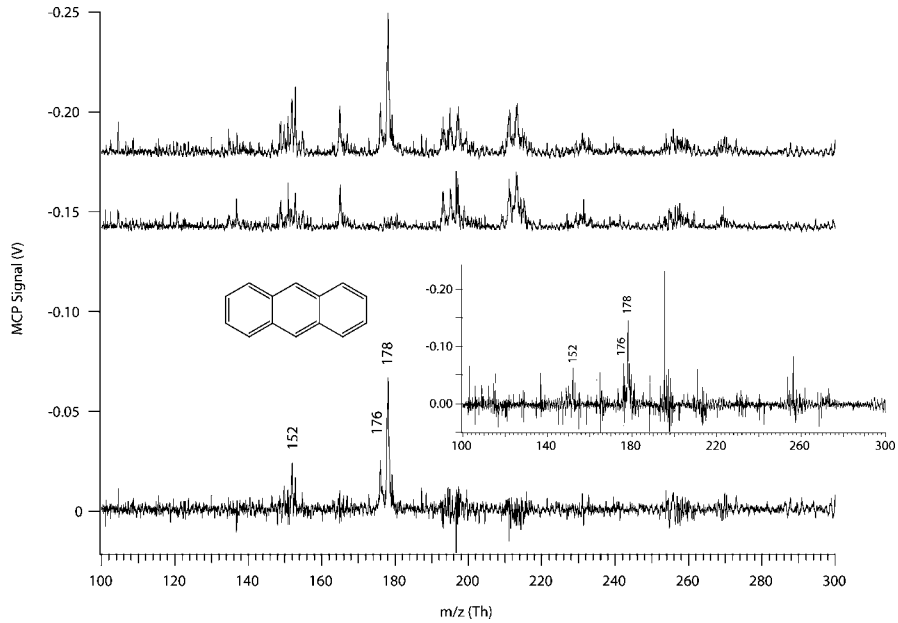


**Figure 4.** Near-field laser ablation mass spectrum recorded on a solid anthracene crystal surface. Bursts of 20 laser shots at 2 kHz, 50 $\mu$J/pulse laser output, were delivered through a SNOM tip, and for every laser burst, an IT-TOF mass spectrum was acquired. Top trace: raw MS signal, averaged over 10 laser ablation bursts/MS acquisitions. Middle trace: background (average of 10 acquisitions). Bottom trace: difference spectrum (background subtracted) of averages, with analyte ions marked. Inset: difference spectrum of a single burst/MS acquisition.

ms, in order to ionize the incoming material. After 10 ms, the ions in the trap were extracted into the TOF region and mass separated. By calibration with reference compounds, the flight times were converted to a $m/z$ scale.

Figure 4 shows the mass spectra acquired. The anthracene spectra were averaged over 10 laser bursts/MS acquisitions. The MS of a single burst/single MS acquisition is also shown (inset in Figure 4). Prominent peaks in the background of the spectra are from the diffusion pump oil and from atmospheric background. By subtraction of the averaged background spectrum, the environmental and instrumental background could be partially removed; this procedure was applied to all other MS data shown in this work. In the resulting background-subtracted spectrum, anthracene is clearly visible with its molecular ion at $m/z$ 178 and typical EI fragments at $m/z$ 176 and 152 (loss of $C_2H_2$). The close positioning of the sampling capillary with respect to the SNOM tip/ablation is crucial: for a successful SNOM-MS experiment, the distance has to be closer than 100 $\mu$m. The limited range of active suction, which is estimated to roughly equal the internal diameter of the sampling capillary (250 $\mu$m), and the limited radius of the laser ablation plume expansion before being stopped by collisions at atmospheric pressure are likely reasons for the need of close positioning. A topographical image after the experiment could not be obtained, since the tip crashed against the sample surface while attempting to scan the topography afterward. It is also possible that debris of material sputtered onto the tip deranged the tip−sample feedback. The anthracene mass spectrum demonstrates that near-field laser ablation at atmospheric pressure and subsequent MS analysis can be performed with the described method.

**Consecutive LA-SNOM on an Anthracene Crystal.** Several topographical images of the sample surface after consecutive ablation events with successful MS analysis for every crater could be obtained for another solid crystal of anthracene. SNOM tips

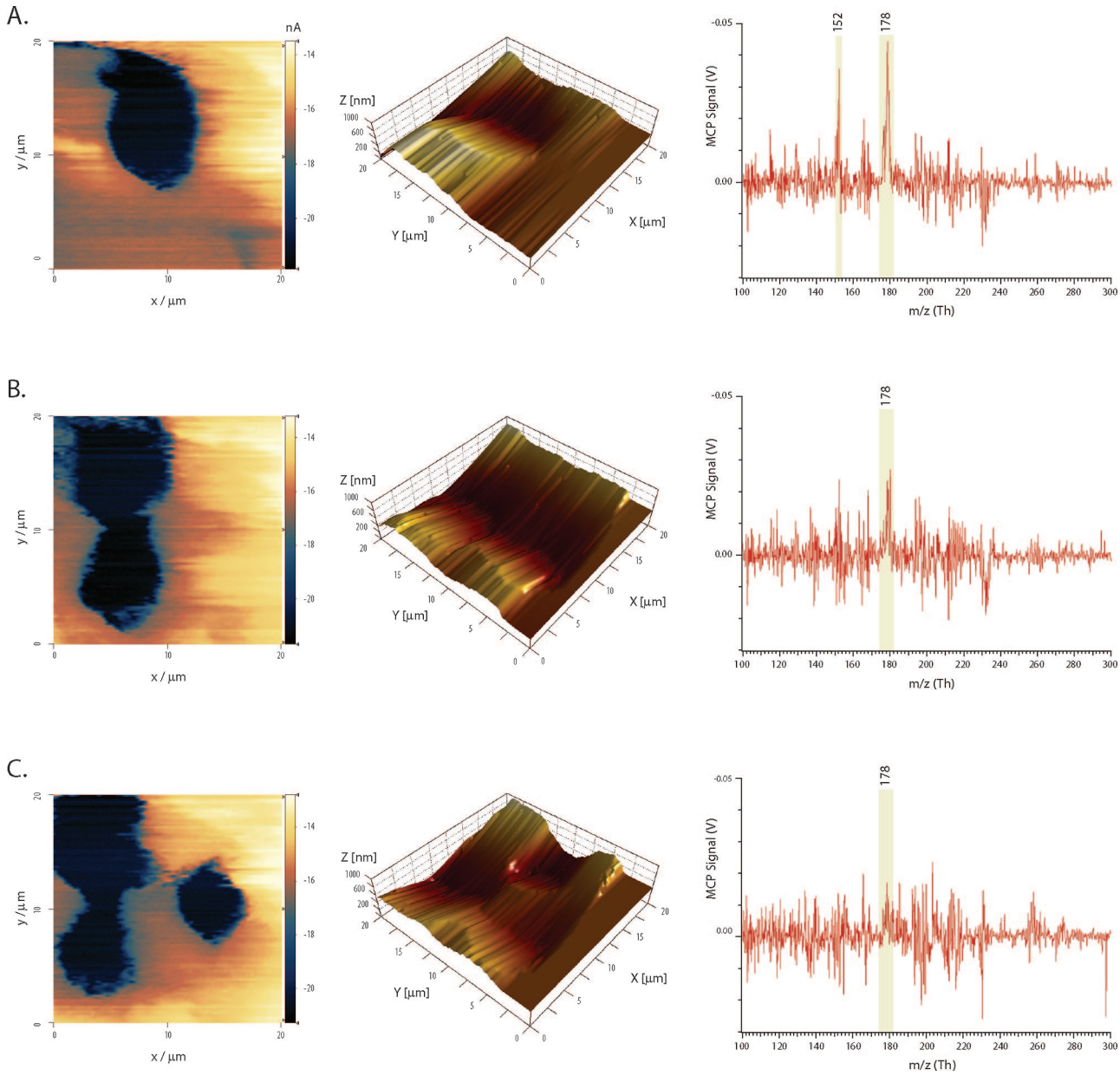


**Figure 5.** Consecutive LA-SNOM-MS analysis of solid anthracene at three different positions (A−C). For every position, a mass spectrum of anthracene could be recorded. The left column displays the acquired *Z*-error signal of the SNOM, which emphasizes edges (similar to a derivative of the absolute height signal). The middle column displays the measured topographical height (*Z*-signal) in a 3D view (scaling is the same for all images). In the right column, the acquired, averaged, and background-subtracted SNOM-MS signal is displayed for every position/crater. The molecular ion of anthracene at *m*/*z* 178 is highlighted; for crater A also the typical EI fragment at *m*/*z* 152 (loss of $C_2H_2$) is visible.

of higher quality, a more precise control of the sampling capillary with respect to the SNOM tip, and better sample mounting (crystal glued to a cover glass) may have improved repeatability for multicrater laser ablation with the same SNOM tip and subsequent scanning of the surface topography. Figure 5 shows three consecutive SNOM laser ablation and surface scans with MS data.

Bursts of 10 laser pulses at 2 kHz were used at a laser power of 30 $\mu$J/pulse. For the first and second craters, 5 bursts were applied, while the last crater was produced with 3 bursts. The diameters of the craters are 13 (Figure 5A), 14 (Figure 5B), and 8 $\mu$m (Figure 5C) and have a fwhm of 8.8 (Figure 5A), 7.9 (Figure 5B), and 5.3 $\mu$m (Figure 5C). From the 3D topography images, it can be seen that displacement of ablated material from the crater to the surroundings by redeposition has occurred (especially visible by comparing Figure 5A with Figure 5B). The estimated amount of ablated material is ~110 (first crater, corrected for the redeposited material on the left side), ~60 (volume of second crater, corrected for the redeposited material on the left side), and ~85 fmol (full volume of third crater) of anthracene. For every burst, a mass spectrum was acquired and averaged over all single-trace mass spectra. The MS spectra in Figure 5A and Figure 5B have S/N ratios of 9.0 and 3.7, respectively. In the case of the last crater, the signal acquired while performing the three bursts was small compared to the background (S ≈ N). However, "tailing" for ~10−20 s after the last ablation event could still be measured with a signal intensity comparable to that of the mass spectrum in Figure 5A. This is in contrast to the first two ablation spots, where such tailing could hardly be observed as the analyte

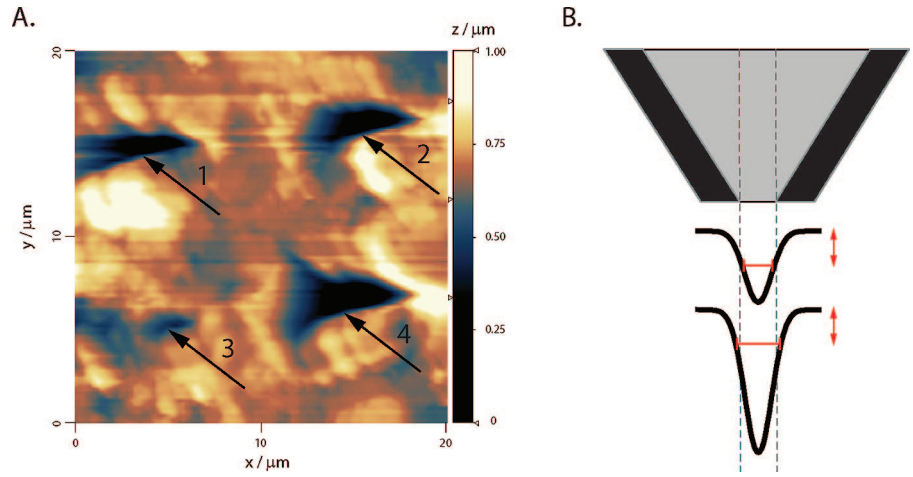


**Figure 6.** (A) Laser ablation crater size "tuned" by the laser power coupled into the SNOM fiber. The ablation experiments shown were conducted with different pulse trains and laser powers, but all with the same SNOM tip. Top left: 5 bursts with 20 shots each, 70 $\mu$J/pulse. Top right: 5 bursts with 10 shots each, 70 $\mu$J/pulse. Bottom left: 5 bursts with 10 shots each, 30 $\mu$J/pulse. Bottom right: 10 bursts with 10 shots each, 70 $\mu$J/pulse. (B) The size of the ablation crater, which is given by the area that experiences an irradiance above the ablation threshold, is dependent on the laser energy emitted by the SNOM tip. By varying the laser power, the crater size can be tuned although the tip aperture size is constant.

signal quickly diminished down to a few percent within the first 10 s after ablation. Our interpretation is that the ablation of the third crater, which was the smallest of all three, generated a fairly large particle of anthracene, which deposited in or near the capillary entrance. Repeated condensation and re-evaporation (by the capillary heat) might explain the delayed observation of the analyte as a "tailing". This suggests that the particle size distribution of ablated material in atmospheric pressure LA-MS was an influence for successful transport and analysis. It also underscores how important good sampling and transport are in order to achieve high detection sensitivity. In fact, the limit of detection of the mass spectrometer is probably better than that stipulated by the measured signal for a given laser ablation crater size, because an appreciable portion of the sample in the form of particles may be unavailable for instantaneous detection, but be observed during the tailing.

**Influence of Laser Sequence on Crater Size.** The crater size produced by SNOM-LA depends on the physical characteristics of the individual SNOM tip (aperture, transmission) and its distance to the sample surface, which can be varied with the SNOM feedback parameters. As demonstrated in Figure 6 in an experiment using a solid crystal of pyrene, the crater size can also be "tuned" by the laser pulse scheme and laser power used.

Using the same laser pulse sequence/irradiation pattern but different laser power affects the crater size to a large extent. This can be seen by comparing the top right with the bottom left crater in Figure 6A. Photothermal or photochemical ablation only occurs if the laser irradiance for a given spot lies over a material-specific irradiation threshold. Because the intensity distribution emitted from a near-field aperture can approximate a Gauss curve, the irradiated area that lies over the ablation threshold is largely dependent on the laser power, which is coupled into the SNOM fiber (schematic representation in Figure 6B). The fact that laser ablation craters can be created with much larger dimensions than the size of a typical SNOM tip aperture is most likely related to thermal heat conduction and melting effects in the solid sample.

Interestingly, it seems that the crater formed does not depend primarily on the number of shots per burst for the same number of bursts applied (laser frequency within a burst is 2 kHz): The crater size for a total number of 100 pulses, delivered by $5 \times 20$ shots (Figure 6, top left), and for 50 pulses, delivered by $5 \times 10$ shots (Figure 6, top right), is roughly the same. On the other hand, a significantly larger crater resulted for a total number of 100 pulses, but delivered by 10 bursts of 10 pulses each (Figure 6, bottom right). Although only a single experimental series is shown here, this was a general observation: the number of bursts is more significant for determining the amount of material ablated than the number of shots per burst. Or put differently, additional laser pulses within the same burst do not seem to contribute to the ablation of significantly more material. As the time lapse from burst to burst is 0.5 s, it seems very likely that the irradiated sample spot can cool down completely between two bursts. At a repetition rate of 2 kHz (500-$\mu$s interval from pulse to pulse), additional heating of the plume by subsequent laser pulses can also be excluded (plume stopping is estimated to occur within 50−150 $\mu$s). The use of laser bursts seems to be a prerequisite for successful SNOM-MS analysis, as no mass spectra could so far be recorded using single laser pulses. Further studies are needed to conclusively support these observations and to develop a theory explaining the observed effects.

The figures of merit demonstrated here for the ion trap/TOF based SNOM-MS are not directly comparable to those obtained by our group in 2001 with the QMS setup.[33] There are several fundamental differences. (i) Choice of analyte: in 2001, nitrogen liberated from photodecomposition of a triazene dimer was measured, which is much easier to sample, ionize, and detect than ablation products from anthracene. In the case of anthracene, redeposition on the sample surface, the SNOM tip,[26] the sampling orifice, and in the transport capillary can occur, which will decrease the overall amount of material available for MS analysis. In addition, a significant fraction of anthracene may be ablated in the form of clusters and particles, which will also not contribute to the MS signal at $m/z = 178$. (ii) Laser parameters: most notably, the 2001 setup used 35-ps pulses, while a 15-ns pulse width was

(33) Stöckle, R.; Setz, P.; Deckert, V.; Lippert, T.; Wokaun, A.; Zenobi, R. *Anal. Chem.* **2001**, *73*, 1399–1402.

used here. The laser pulse width may influence the resulting particle size distribution and redeposition of material. Laser parameters are not expected to decrease the sensitivity for the detection of $N_2$. (iii) Transport: the 2001 setup used a direct interface between atmospheric pressure and vacuum, while the current setup uses differential pumping. While the larger capillary diameter (250 $\mu$m) prevents clogging, the total transmission for the analyte is relatively low, estimated to be only ~2% based on gas flow measurements and enrichment factors determined for the skimming process. (iv) Mass analyzer: in contrast to the QMS used in 2001, the ion trap/TOF should have an better overall sensitivity for the same number of ions, as it should achieve a better S/N ratio due to ion accumulation before detection. On the other hand, fragmentation of ions by in-trap EI can decrease the amount of intact analyte molecular ions.

## CONCLUSIONS

An instrument combining SNOM and mass spectrometry was built, and the feasibility for spatially resolved, mass spectrometric analysis of molecular solids was demonstrated. Near-field laser ablation MS at atmospheric pressure with full mass spectral information could be shown for the first time, with a lateral resolution on the low-micrometer scale. No other technique available today offers the same kind of chemical information with such spatial resolution at atmospheric pressure; topographical analysis with nanometer resolution is available at the same time. In principle, crater sizes down to 100 nm can be achieved with the same SNOM-LA technique. The spatial resolution of the method is at present mostly limited by the sensitivity of the mass spectrometer, given by compromises in transport and ionization efficiency. Redeposition of ablated material has not been investigated but may also play a role. It may lead not only to smaller amounts of sample available for analysis but also to spot-to-spot cross-contamination, smearing out the spatial resolution. Numerous possibilities for improvement still exist. (i) Ablation conditions have to be further optimized such that the formation of neutral gas-phase species or very small clusters (<10 nm) is maximized, while minimizing the formation of large particles that may never reach the ion trap or may be redeposited on the surface. (ii) Ionization efficiency should be further improved. The in-trap EI ionization is suspected to lower sensitivity due to fragmentation. Space-charge problems originating from the ions formed from the abundant atmospheric background may also be an issue: although not trapped, nitrogen and oxygen ions will continuously be formed and pass through the ion tap. The use of a softer ionization source, such as photoionization, could alleviate this problem. While in-trap ionization avoids ion transmission losses, ionization outside of the trap might be overall more efficient. (iii) Sampling of the ablated neutral molecules is probably the best approach, although our SNOM-LA instrument could also be used with an atmospheric postionization technique (radioactive source, corona discharge, APCI). However, this would require custom-made ion optics to sample, transport, and guide the ions over a relatively large distance into the mass analyzer. Efficient trapping for this mode of operation would also be more problematic. Our emphasis is therefore to improve the ionization efficiency in the trap and the sampling and transport efficiency.

As an extension of the demonstrated SNOM-MS concept, additional chemical contrast mechanisms could be added, such as fluorescence imaging of labeled biological compounds. By choosing a suitable laser wavelength for a given fluorophore, the sample could be analyzed in five dimensions (3D topography, mass spectrometry, and fluorescence). A single-point mass spectrum requires a time of 50−100 ms for analyte transport, analysis, and trapping; thus, a 100 × 100 pixel image will require ~8−16 min for chemical (and topographical) imaging. Although competing methods such as SIMS or stigmatic ion imaging are faster, the time required for suitable high-vacuum sample preparation and sample introduction has to be taken into account as well. Therefore, this method has the potential to become a useful tool for nanoanalysis, especially for biological systems. Instead of a UV laser, a mid-IR laser that is absorbed by water could be used for matrix-free, in situ analysis of biological tissue samples at atmospheric pressure with high spatial resolution. This could be accomplished with IR-transmitting SNOM tips[34,35] and an appropriate pulsed IR laser source.


## ACKNOWLEDGMENT

The authors thank D. Tonoli for preparing the pyrene crystals. Technical support from K. Baumgartner, H. Benz, and R. Dreier and are greatfully acknowledged. SEM images were taken with the assistance of Dr. F. Krumeich at the Electron Microscopy Centre at ETH Zurich (EMEZ). This work was supported in its early phase by the GEBERT RÜF STIFTUNG (Grant P-085/03).


## NOTE ADDED AFTER ASAP PUBLICATION

The title of this paper published ASAP July 12, 2008 was modified; the corrected version published ASAP July 25, 2008.


Received for review March 10, 2008. Accepted June 9, 2008.

AC8005044



(34) Hong, M. K.; Erramilli, S.; Huie, P.; James, G.; Jeung, A. *Proc. SPIE* **1996**, *2863*, 54–63.

(35) Schaafsma, D. T.; Mossadegh, R.; Sanghera, J. S.; Aggarwal, I. D.; Gilligan, J. M.; Tolk, N. H.; Luce, M.; Generosi, R.; Perfetti, P.; Cricenti, A.; Margaritondo, G. *Ultramicroscopy* **1999**, *77*, 77–81.